

Properties of 3D HI Filaments in the Smith High Velocity Cloud

Colin Holm-Hansen,¹ M. E. Putman,² D. A. Kim²

¹*Department of Physics, Columbia University, New York, NY 10027, USA*

²*Department of Astronomy, Columbia University, New York, NY 10027, USA*

Accepted XXX. Received YYY; in original form ZZZ

ABSTRACT

We present findings of 3D filamentary structures in the Smith Cloud, a high-velocity cloud (HVC) located at $l = 38^\circ$, $b = -13^\circ$. We use data from the Galactic Arecibo L-Band Feed Array H I (GALFA-H I) along with our new filament detection algorithm, `fil3d`, to characterize these structures. In this paper, we also discuss how different input parameters affect the output of `fil3d`. We study filaments in the local ISM and compare them to those found in the Smith Cloud. Based on thermal linewidth estimations we find supporting evidence that the Smith Cloud filaments are part of its warm neutral medium. We also find a relationship between thermal linewidth and the v_{LSR} of the filaments. We study the plane-of-sky magnetic field as traced by Planck 353 GHz polarized dust emission along the line of sight and find the HI filaments in this region are not aligned with the magnetic field. This is likely related to their location close to dynamic processes in the Galactic Plane and/or the low column density of the filaments relative to emission in the Plane. The results show the HI filaments are found in a wide range of Galactic environments and form through multiple processes.

Key words: ISM:clouds – ISM:kinematics and dynamics – ISM:structure

1 INTRODUCTION

The interstellar medium (ISM) is flush with complex morphology. It has been shown that there exists an intricate network of molecular filaments that may be linked to star formation (e.g., André et al. 2014). Recently, H I filaments have also been found at varying Galactic scales (McClure-Griffiths et al. 2006; Clark et al. 2014; HI4PI Collaboration et al. 2016; Kalberla et al. 2016; Soler et al. 2020, 2022). Unlike molecular clouds, these objects are not self-gravitating, meaning they must form due to factors in their environment. Given that they have been detected in several environments at varying scales and densities, multiple formation mechanisms may exist. In order to understand their formation, a plethora of work has been underway studying their physical properties. It has been shown that these filaments tend to align with the ambient magnetic field traced by polarized dust emission (McClure-Griffiths et al. 2006; Clark et al. 2014; Kim et al. 2023). Around the Galactic plane, alignment is mostly parallel to the plane, but due to several factors smaller regions with perpendicular planar alignment are also present (Soler et al. 2020, 2022).

Characterization of filaments in regions beyond the local ISM is beginning to take shape as well. Ma et al. (2023) studied filamentary structure in regions of the Small Magellanic Cloud and found possible evidence of alignment with its magnetic field. Jung et al. (2023) has shown in MHD simulations that high-velocity clouds (HVCs) draped in a magnetic field should have filaments along their direction of motion. However, up until now, the quantification of observed H I filaments in a HVC has not been done.

The Smith Cloud (Smith 1963) is one of the most thoroughly studied HVCs with a known distance of 12.4 kpc (Putman et al. 2003; Lockman et al. 2008; Wakker et al. 2008). Like other HVCs it

has a comet-like morphology with a compact head and more diffuse tail. Its head is located at approximately $l = 38^\circ$, $b = -13^\circ$, and the whole structure extends approximately 1×3 kpc across the sky. Mass estimates place it having around $10^6 M_\odot$ in both neutral H I and H II (Lockman et al. 2008; Hill et al. 2009). Its magnetic field strength has been mapped using Faraday Rotation (Hill et al. 2013; Betti et al. 2019). Lockman et al. (2008) computes a z-height for the Smith Cloud of -2.9 ± 0.3 kpc, which we adopt for this paper. Kinematic analysis done by Lockman et al. (2008) has shown that it is on a trajectory toward the Galactic plane and will reach it in about 30 Myr.

The origin of the Smith Cloud is still unknown. It has been proposed as having an extragalactic origin (Bland-Hawthorn et al. 1998) or a local origin as a conglomerate ejected from the disc of the Milky Way (Sofue et al. 2004; Marasco & Fraternali 2017). If it is a failed dwarf galaxy it likely already passed through the disc approximately 70 Myr ago and in order for it to have survived this encounter it must have a dark matter halo (Nichols & Bland-Hawthorn 2009). If it has a local origin, Alig et al. (2018) has shown that this encounter with the disc may trigger a burst in star formation in the disc gas.

In this paper, we investigate the structure and properties of 3D H I filaments in the Smith Cloud. We compare their properties to filaments at lower velocities along the same line of sight. Section 2 introduces the data and reviews the procedures for both extracting and analyzing 3D H I filaments using our 3D Filament finding algorithm, `fil3d`. Section 3 discusses the effects of `fil3d` parameters on the final filament populations and goes over the selections made for this study. Section 4 shows the results when applied to the data and investigates filament properties such as physical characteristics and

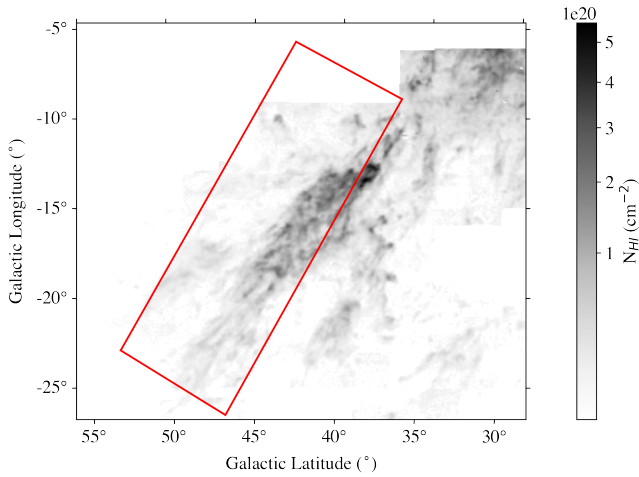


Figure 1. The Smith Cloud as shown in Lockman et al. (2008) integrated from 70–130 km s^{−1} with the column density from the moment 0 map shown with the right scale bar. The GALFA-H I region is shown in a rectangle outlined in red.

magnetic field orientation. We discuss these results and present our conclusions in Section 5.

2 DATA & METHODS

We extract filaments with data from the Galactic Arecibo L-Band Feed Array H I (GALFA-H I) survey (Peek et al. 2018). GALFA-H I is highly effective at locating filaments due to its sensitivity and spatial resolution of 4′. The data are gridded to 1′ × 1′ pixels. We downloaded a custom cube from the GALFA-H I website, using the 0.739 km s^{−1} channel spacing for spectral resolution over a total velocity range of $-68 < v_{LSR} < 188$ km s^{−1}. The upper-velocity range for the cube was selected to ensure that the entire extent of the Smith Cloud would be captured. The RMS noise is 150 mK per 1 km s^{−1} velocity channel. The total region of sky sampled is $292^\circ < \alpha < 312^\circ$ and $-1^\circ < \delta < 6^\circ$. The trade-off with using the high spatial resolution GALFA-H I data over other survey data is that we are located at the minimum declination of GALFA-H I’s observation region ($-1^\circ 17'$), whereas the main component of Smith Cloud extends as far as -2° (see Lockman et al. 2008). Figures 1 and 2 show the entire Smith Cloud as shown in the GBT (Lockman et al. 2008) and the GALFA-H I region respectively. For magnetic field information, we employ the *Planck* 353 GHz Stokes linear polarization maps (Planck Collaboration et al. 2020). We smooth the resolution of the *Planck* maps to a full width at half-maximum (FWHM) of 1° from their original resolution of 4.9′ in order to improve the maps’ signal-to-noise ratio.

We use the *fil3d* algorithm to identify filaments in GALFA-H I as discussed in Kim et al. (2023) and Putman et al. (in prep.). In an attempt to capture the entirety of the Smith Cloud, we also tried running *fil3d* on data from the Robert C. Byrd Green Bank Telescope (GBT) from Lockman et al. (2008) as well as from the H I 4π survey (HI4PI Collaboration et al. 2016) using a wide range of settings, but found with the larger beamwidths (10′ and 16′, respectively), filaments are not resolved enough to be captured by *fil3d* (although see Figure 3 for the 2D filament map using the GBT data). We follow the same procedure for extracting filaments laid out in Kim et al. (2023) and Putman et al. (in prep.), which can be consulted for more details.

We begin by applying an unsharp mask (USM) with a 30′ Gaussian beam to each channel in the spectral cube, which acts as a high-pass filter, removing diffuse emission. Following this we run *filFinder* (Koch & Rosolowsky 2015) to identify 2D filamentary structures in each channel. Each 2D filament is referred to as a node. If any two nodes in adjacent channels share 85% of pixels in common, they are considered to be part of one composite 3D object, known as a tree. Once a tree is formed, it is finalized by repeating this process until adjacent channels have no significant overlap. The final mask for a tree is the aggregated mask of each of its nodes, called the merged mask.

After generating trees, we validate them based on several criteria. First, only trees with an aspect ratio of 1:6 or greater are accepted to ensure filament-like morphology. Since *filFinder* tends to pick up more noise at the edges, any trees with a merged mask along the edge of the data are also discarded. If filaments pass these first two criteria we inspect their median intensity within the merged masked area as a function of their velocity (see Kim et al. (2023), figure 4). This is done since most *fil3d* trees only span 2–3 channels. As such, we consider the entire Gaussian profile to be a more physical line width for the filaments as opposed to only the *fil3d* detected channels. To ensure the validity of this assumption, we require that the median velocity channel detected by *fil3d* falls within one standard deviation of the best fit Gaussian profile. Finally, we visually inspect the merged mask contours overlaid on a moment zero map of the USM data integrated over the FWHM of their Gaussian profile. Since we are interpreting this range as the true linewidth of a filament, we require that the moment zero map integrated over this range be consistent with the original *fil3d* merged mask. Therefore, only filaments whose merged masks match the data over their FWHM range are accepted. Filaments that pass all of these criteria are then saved in the final set. Applying this to our dataset we find an initial return of 135, which becomes 72 after the filtering process. The final batch covers a velocity range (taken to be the velocity of the median channel of the filament found by *fil3d*) of $-6 < v_{LSR} < 107$ km s^{−1}.

For the plane of sky magnetic field data, we follow the same procedure as Kim et al. (2023), using the supplied Stokes data to obtain the dust polarization ψ in the Galactic IAU convention. Since polarized dust grains align perpendicularly with the ambient magnetic field, we define the plane of sky magnetic field orientation ϕ at a given location to be:

$$\phi = \frac{1}{2} \arctan(U, -Q) \quad (1)$$

which is a 90° rotation from ψ . From this, we compute the the average B-field value $\bar{\phi}$ in the area of each filament:

$$\bar{\phi} = \frac{\sum_j \sum_i \phi(x_i, y_j)}{A} \quad (2)$$

where A is the area of the merged mask, and $\phi(x_i, y_j)$ is the magnetic field orientation at location (x_i, y_j) within the area of the merged mask. The orientations of the filaments themselves, denoted as θ , are computed using the Rolling Hough Transform (RHT) as described in Clark et al. (2014). We define the difference between these two values, $|\theta - \bar{\phi}|$, to be the mean magnetic alignment of a filament. We also compute the polarization fraction p for each filament:

$$p = \frac{\sqrt{U^2 + Q^2}}{I} \quad (3)$$

which we use to help discuss our findings in Section 5.

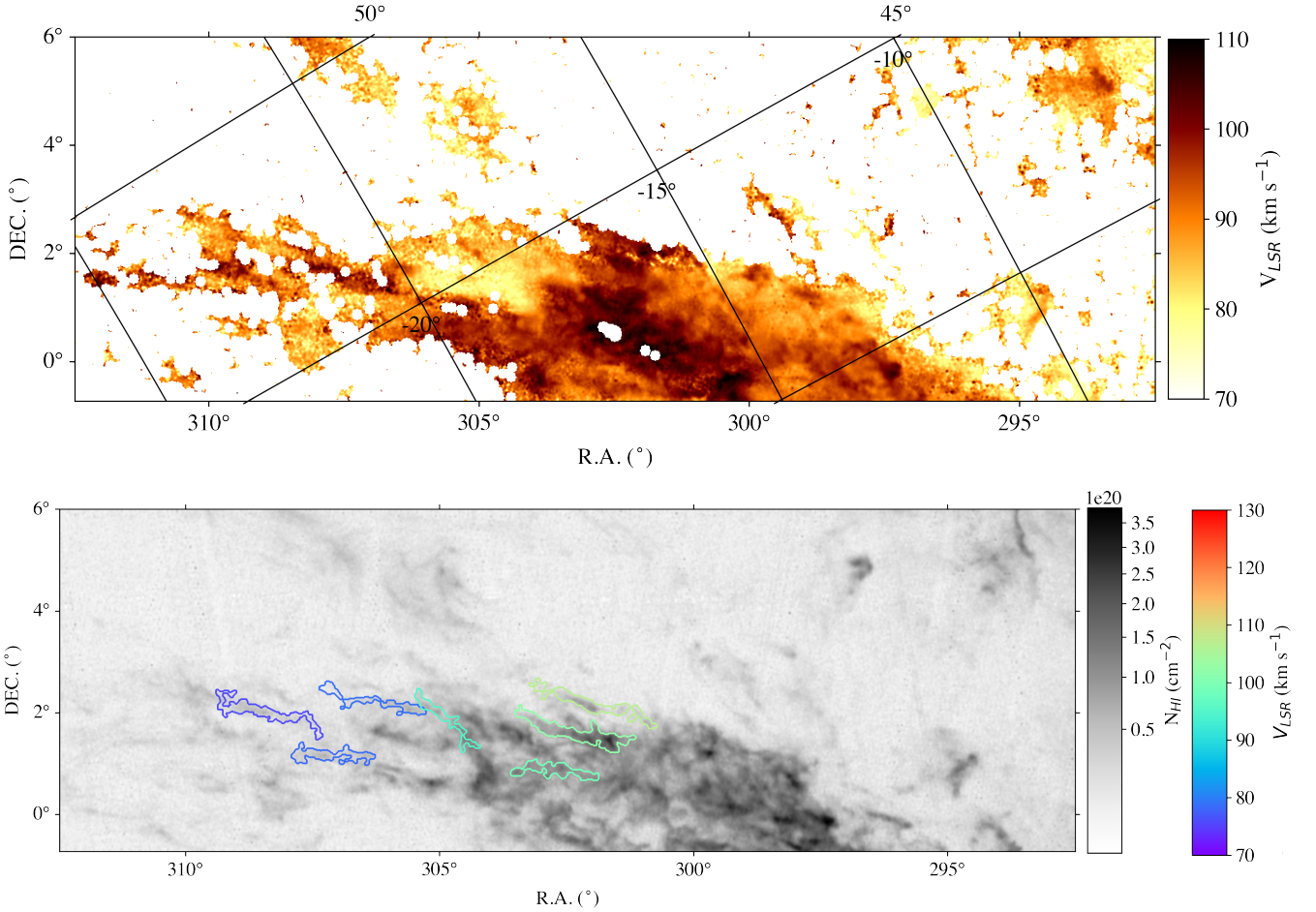


Figure 2. Top: Average velocity moment 1 map of the GALFA-H I region of the Smith Cloud over the same velocity range as Figure 1 with Galactic coordinates overlaid. Bottom: Filament masks overlaid on N_{HI} map of the Smith Cloud integrated from 70-130 km s^{-1} . The vertical lines present in the background are artefacts from the basketweave scanning method used for GALFA-H I.

3 FIL3D DEPENDENCIES

The output generated from `fil3D` is sensitive to its multiple input parameters, including inputs made to `Filfinder`, the overlap percentage, the aspect ratio filter, and the width of the USM Gaussian kernel. Different inputs should be expected to work better for different data sets as well as in different regions. Overall, we find that tweaking these parameters often changes the total number of filaments, but the overall trends and findings discussed in Section 4 stay the same. Here we discuss the selections made for this study. For these selections, we find the multiple steps of validation criteria to serve as a means to minimize artefacts in the final population. For example, lowering the size threshold or the minimum aspect ratio requirement inherently leads to more junk being included in the initial return sample. However, we find that when these changes are made, the percentage of filaments removed by the velocity filter increases significantly. As such, the multiple criteria help ensure the validity of the final population.

3.1 Filfinder Parameters

The nodes drawn from each channel are partially dependent on the parameters used for `Filfinder`. For these, we start by defining a

characteristic `scale_width` and defining the rest of our variables with respect to it. For this value, we found 0.1 pc to work the best. 0.15 pc and 0.05 pc were also tried, but with the former, the number of filaments drops drastically and the latter picks up too many artefacts. Other inputs to `Filfinder` include `smooth_size` which was set to $0.5 * \text{scale_width}$, and `adaptive_threshold` which was set to $2 * \text{scale_width}$. `smooth_size` determines the magnitude of the beam applied to the image to remove small noise variations, and `adaptive_threshold` is a parameter related to the expected filament size. `border_masking`, which excludes the edges from the search region, was set to false. More details on these parameters can be found in the `Filfinder` documentation.

The `Filfinder` parameter that was given the most consideration was `size_threshold`, which is the minimum size required for an individual node to be considered real. We experimented with using both very large and very small values for this parameter. We started with $8 * (\text{scale_width} * 2)^2$ (used in Kim et al. (2023) and Putman et al.), but found that this left out visibly filamentary structure in the Smith Cloud. We then tried dropping it down to 5 pix^2 with the thought that any junk picked up would be filtered out through our other validation criteria. However, we found that under this setting many filaments ended up with nodes only a few pixels in size, and some filaments recovered at higher size thresholds had additional

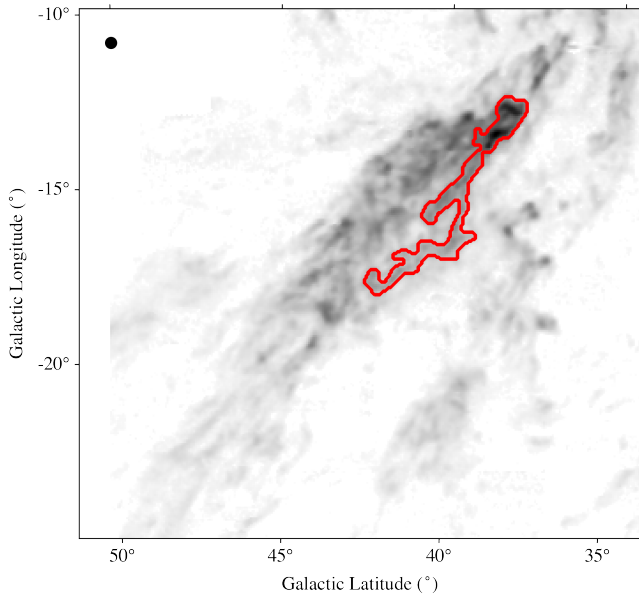


Figure 3. Filfinder results ran on the moment 0 map in Figure 1 with a 1:2 aspect ratio cut, minimum area of twice the beam size, and edge filtering applied. The prominent structure centered at $(l,b) \approx (40^\circ, -15^\circ)$ is outside of the GALFA-H I data.

nodes at the beginning or end of their channels that were squares 5-10 pixels in size. We eventually settled on $3 \times (\text{scale_width} \times 2)^2$ as a compromise between the two extremes. The smallest nodes were inspected visually at this threshold and none appeared to be artefacts.

3.2 Aspect Ratio

We tested several different aspect ratio filters: 1:6, 1:5, 1:4, and even 1:2 was considered to better understand the overall effect on the final filament count. As expected, as the aspect ratio filter drops, the total number of filaments increases. For these data, 1:6 usually returned just under one hundred filaments (For this subsection, the totals referred to do not include any other sort of filtering as discussed in Section 2 other than the aspect ratio filter). 1:5 and 1:4 returned several hundred filaments each, and 1:2 returned over one thousand filaments. As with other parameters, these aspect ratio outputs were inspected visually to determine which produced the most filaments without producing too many artefacts. We selected 1:6 for this study, consistent with what was used in Kim et al. (2023) and Putman et. al (in prep).

3.3 Overlap Threshold

We find the ability to vary the overlap threshold is somewhat limited. Somewhat counter-intuitively, the total number of filaments found decreases if the overlap threshold is lowered too far below 85%. This occurs because as the overlap threshold is lowered, more and more nodes are accumulated into the merged mask structure. This causes filaments to span across more channels on average, but it also causes them to become wider, or to pick up adjacent material that is not associated with them. As such their aspect ratios decrease, causing more filaments to be rejected by the aspect ratio filter. For this region we found this to start occurring at an overlap threshold of 65%.

3.4 Resolution

To illustrate the dependency of spatial resolution in this section we compare the Filfinder output on moment 0 maps integrated from 70-130 km s^{-1} for both the GBT and GALFA-H I data. For each output, we apply a rough filter of a minimum aspect ratio of 1:2, a minimum size of twice the beam size, and remove any filaments that touch the edge of the data. We apply a smaller aspect ratio filter here since the Filfinder output of a single channel is more comparable to a node which is smaller on average than a tree, meaning the corresponding node aspect ratio is smaller. The outputs are shown in Figures 3 and 4 respectively. The GBT data only returns one object satisfying these criteria along the lower ridge of the body of the Smith Cloud, which is located in a region outside of the GALFA-H I data. This motivates why we were unable to find filaments in the GBT data. By contrast, the GALFA-H I data returns 70 structures (although artefacts are definitely still present), and there are cohesive filament structures at the locations of fil3d trees.

The different spatial resolutions also correspond to different width scales. For GALFA-H I structures that Filfinder can compute the width of, i.e. excluding artefacts and other structures with obscure geometries, the average width is 32.9 pc at a distance of 12.4 kpc. By contrast, the computed width of the GBT structure in the lower ridge of the Smith Cloud body is 107.9 pc.

4 RESULTS

We find a total of 72 filaments passing all criteria outlined in Section 2. Looking at the distribution of median velocities for each filament as shown in Figure 5, we categorize the filaments into three distinct groups. The bulk of filaments with median velocities less than 20 km s^{-1} are considered to be relatively local structures in the Galactic disc. The second group is a smaller population between 20 and 70 km s^{-1} , which are largely thought to represent structures in intermediate velocity clouds (IVCs). The remaining group, all with velocities of 70 km s^{-1} or greater, are the filaments located in the Smith Cloud. This range of velocities for the Smith Cloud is based on Figure 3 of Lockman et al. (2008), which suggests that prominent Smith Cloud flux ranges from 70-130 km s^{-1} . The HVC filaments are plotted in Figure 2. The entire group of filaments are plotted in Figure 6.

The magnetic field alignment of filaments is shown in Figures 6 and 9. The color indicates $|\theta - \bar{\phi}|$ for each filament in degrees. The local filaments appear preferentially anti-aligned, with a median alignment of 59.7° and a mean of 56.3° . The anti-alignment falls off going to higher velocities, and for the IVC and HVC population, the filaments seem to be more randomly oriented with respect to the Planck data. The median B-field alignment, as well as a summary of overall attributes for each group, are shown in Table 1. The mean computed polarization fraction within the merged mask area of the local filaments is .0725.

We make a temperature estimate for each filament by the following relation between gas line width and temperature:

$$T = 21.9 \text{ K} \left(\frac{\Delta v}{\text{km s}^{-1}} \right)^2 \quad (4)$$

where Δv is the FWHM as discussed in Section 2. FWHM as a function of median filament velocity is plotted in Figure 7. The median temperature of the local filaments is 203 K, indicating they are part of the cold neutral medium (CNM). The median HVC population temperature is ~ 7400 K and the mean is ~ 9300 K. This is expected

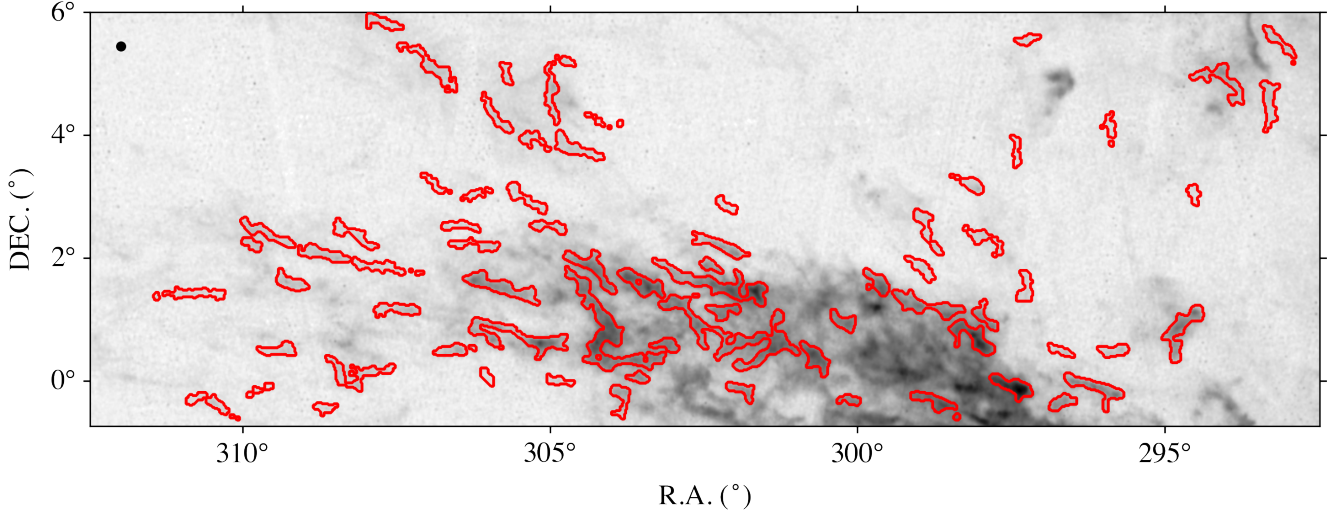


Figure 4. Filfinder results ran on the moment 0 map of the GALFA-H I region for comparison with Figure 3. The beam size is drawn as a black circle in the upper left corner.

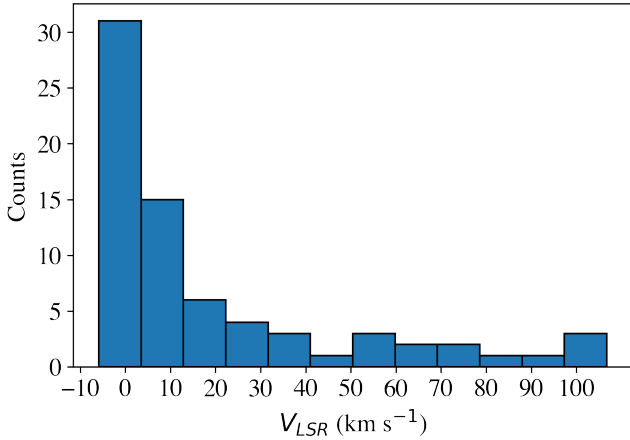


Figure 5. Histogram of the final sample of 3D filaments as a function of their median fil3d v_{LSR} .

since the Smith Cloud is known to have a warm neutral medium (WNM) and has been shown to have a H II mass comparable to its H I mass (Putman et al. 2003; Hill et al. 2009). In particular, Hill et al. (2009) placed a lower bound temperature estimate of 7000 ± 2000 K, which these results are consistent with. Apparent from the graph is a correlation between velocity and temperature of the H I gas along this line of sight.

We also examine the column density of each filament. We evaluate the column densities by integrating over the FWHM of the line width fitted to each filament as discussed in 2. Figure 8 shows the median column density within the merged mask area of each filament as a function of that filament’s velocity for both the raw and USM data. The raw data shows a maximum density at $v_{LSR} \approx 0$ km s⁻¹ followed by an exponentially decreasing relationship out to higher velocities. We interpret this as a result of the fact that along this line of sight increasing v_{LSR} corresponds to increased distance from the Galactic disc. More details on filament column densities, as well as filament spatial widths, are discussed in Putman et. al. (in prep.).

Table 1. Properties for each filament group. The median value is reported for the B-field alignment, FWHM, and temperature.

Group	N	Velocity Range (km s ⁻¹)	$ \theta - \bar{\phi} $ (°)	FWHM (km s ⁻¹)	Temp. (K)
Local	52	-8-20	59.7	3.05	203
IVC	13	20-65	47.2	10.1	2240
HVC	7	75-110	77.3	17.8	6900

The majority of filaments detected in the Smith Cloud itself are located away from the head, closer to the tail and midsection. Looking at Figure 3, it seems probable there are more filaments in the midsection that are not being detected due to them being partially or completely cut off from the GALFA-H I region. Moreover, such filaments would be at the edge of the region where *fil3D* tends to pick up noise. The filaments that are detected are aligned with the morphology of the Smith Cloud itself. There are initially 9 detected after filtering in this region; however, there was a significant overlap in the filament contours for two filaments in the tail and two in the body. We inspected the nodes for these trees and found that in each case the last node of the first tree and the first node of the second tree were in adjacent channels with an overlap fraction of 80% and 75% respectively, just below our threshold of 85%. Given that their contours along the long axis of the filaments were nearly identical, combined with the greater thermal broadening in this region, we merged these tree groups into one filament each, leaving 7 trees in the region in total.

We attempted to investigate the dust content of the Smith Cloud with the *Planck* 857 GHz data. We created a map of the dust emission expected in this region from the Galactic emission alone by creating a column density map integrated from -60 km s⁻¹ < v_{LSR} < 60 km s⁻¹ and multiplying by the $I_{857}/N_{H I}$ ratio from Planck Collaboration et al. (2014). We then subtracted the expected map from the *Planck* 857 GHz map to create a residual map. Figure 10 shows these maps and that there appears to be a visual excess in the region of the Smith Cloud in the residual map. The excess in this map at the level of 0.5 MJy/sr was confirmed by randomly sampling 1000 on and off points and using a 2-sample T-test, however, there are too

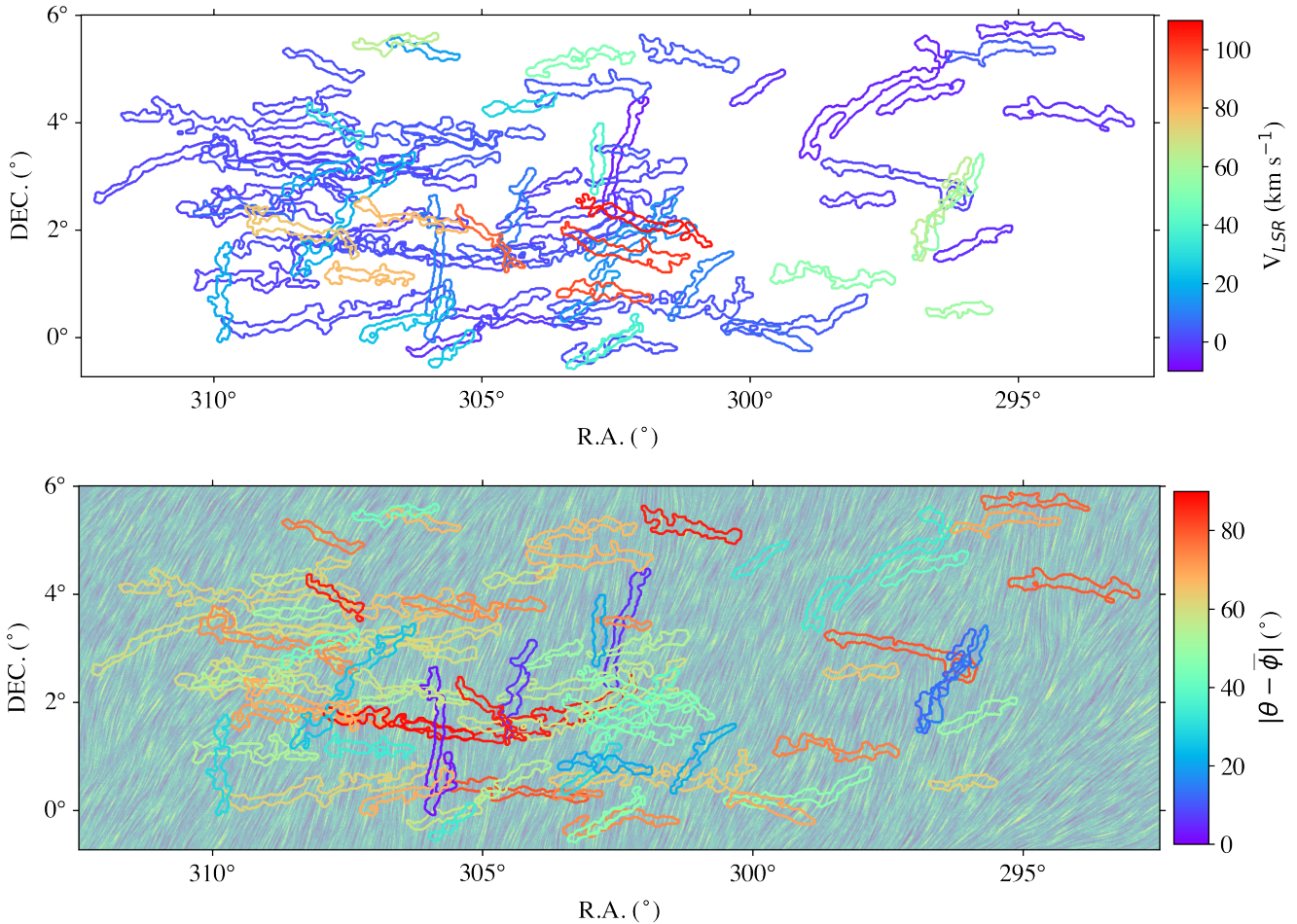


Figure 6. Top: Catalog of all filaments detected. Color indicates v_{LSR} of the median channel of the filament as found by `f113d`. Bottom: Magnetic field orientation of all filaments. The background shows magnetic field orientation drawn with line integral convolution. Local filaments appear anti-aligned in this region.

many caveats to claim this excess is directly from the Smith Cloud. Tests of additional regions are needed and the residual map is positive over the majority of the map indicating the scaling ratio from [Planck Collaboration et al. \(2014\)](#) was not a good fit in this region. This makes sense given the low Galactic latitude of this sight-line and shows that caution is needed when producing expected FIR maps with this ratio.

5 DISCUSSION

We present the first findings of velocity-resolved 3D H I filaments in an HVC. We also identify local filaments with a preferential orientation perpendicular to the plane-of-sky magnetic field. Here we discuss both findings.

5.1 Local 3D Filaments

Overall the local filaments are consistent with the 3D filaments detected by [Kim et al. \(2023\)](#) at high Galactic latitude. The distinct exception is the filaments in this low Galactic latitude region are mostly anti-aligned with the plane-of-sky magnetic field. To further confirm this result, we compared our findings to the H I orientations

in the Clark & Hensley maps ([Clark & Hensley 2019](#)). Using the same procedure that was done to compare alignment with the *Planck* 353-GHz polarization map, we compute a median alignment between our 3D local filaments and the C&H map of 15.7° , indicating a strong alignment. We also checked our magnetic field results from Planck by comparing it with the magnetic field derivation in [Soler et al. \(2016\)](#) and found our model matches their findings.

Filaments that are perpendicular to the Galactic magnetic field near the plane have previously been detected in [Soler et al. \(2020\)](#) and [Soler et al. \(2022\)](#), which looked for H I filaments at $|b| < 1.25^\circ$ and $|b| < 10^\circ$, respectively. They associate regions of perpendicular alignment with H II regions and supernovae feedback from the Galactic fountain ([Shapiro & Field 1976](#); [Putman et al. 2012](#)). In particular, [Soler et al. \(2022\)](#) finds more perpendicular filaments toward the inner galaxy, which also makes sense if caused by the Galactic fountain since there is a greater concentration of supernovae remnants in the inner galaxy (e.g., [Green 2015](#)). This is consistent with our findings, since the region studied here points toward the inner galaxy in the direction of the Sagittarius Arm. The local filaments in our sample are also preferentially oriented perpendicular to the Galactic plane.

Our local filament properties can be compared to [Kim et al. \(2023\)](#), which observed a H I filament population at high Galactic latitude. While we find a different behavior with respect to the magnetic

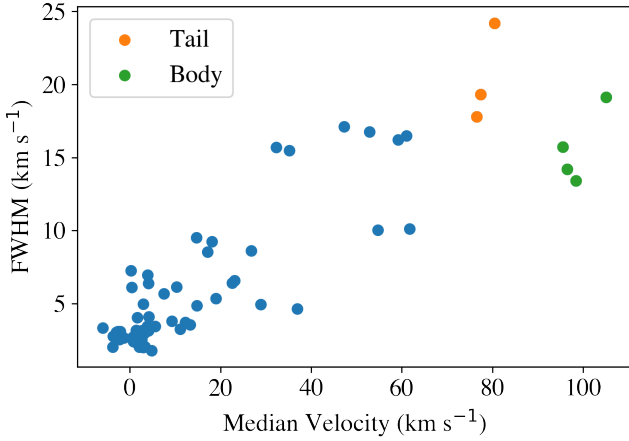


Figure 7. FWHM as a function of median velocity. Points located in the tail of the Smith Cloud are in orange while points in the tip are in green. Filaments not in the Smith Cloud are blue.

field, we find a mean linewidth of 3.72 km s^{-1} and median column density of $10^{19.9} \text{ cm}^{-2}$, compared to their findings of 3.1 km s^{-1} and $10^{19.6} \text{ cm}^{-2}$, respectively. Our somewhat greater line-width may be influenced by the fact that we employ a velocity resolution of $.739 \text{ km s}^{-1}$ in the GALFA-H I data whereas Kim et al. (2023) uses the narrower channels with a $.184 \text{ km s}^{-1}$ resolution. Our slightly greater column density value makes sense as well in the context of our filaments being located closer to the Galactic plane. That being said, the column density of all of our filaments (Figure 8) is still low compared to the general Galactic HI (above 10^{21} cm^{-2}). Since the dust along this line of sight is likely associated with the densest HI, the HI filaments detected here may not be tracing exactly the same material as the *Planck* data. This could then also explain the lack of alignment with the Galactic magnetic field.

5.2 HVC Filaments

We find 7 filaments in the HVC known as the Smith Cloud, and they are oriented along its long axis. There is no consensus reason for how filaments form, given their presence at varying scales and environments (Hacar et al. 2023). As the Smith Cloud approaches the Galactic disc, it encounters greater and greater pressure from the surrounding medium. At the same time, ram pressure stripping of the cloud ablates material, creating fragments that are potentially condensed by the surrounding medium (Heitsch & Putman 2009). It is already known that the head-tail structures of HVCs have more elongated lower-density structures in the tail (Quilis & Moore 2001; Heitsch & Putman 2009). Such conditions are more conducive to filament formation and may be consistent with warmer filaments towards the trailing tail of the HVC.

The HVC magnetic field may also play a role in the filament formation. Previous work has shown local H I filaments at higher Galactic latitudes align with the plane of sky magnetic field as traced by dust polarization (Clark et al. 2014, 2015; Kim et al. 2023), but to what effect the magnetic field plays in the formation of the filaments is less certain. While we find the IVC and HVC filament alignment to be randomly oriented in regard to the magnetic field traced by 353 GHz dust polarization along the line of sight, the local ISM dominates the dust column with respect to the IVC dust (Panopoulou et al. 2019). Given the non-detection or limited detection of dust in

HVCs (e.g., Peek et al. 2009; Lenz et al. 2017), it is reasonable to assume that the *Planck* data does not capture IVC and HVC magnetic field information. Recent estimates of the field strength for the Smith Cloud’s magnetic field place it at $5 \mu\text{G}$ (Betti et al. 2019), making its influence on its local environment substantial. Furthermore, Betti et al. (2019) created a model magnetic field for the Smith Cloud that would give a magnetic field orientation along the long axis of the Smith Cloud. Since this is the same orientation as our detected Smith Cloud filaments, they are potentially aligned with its local magnetic field.

The line widths of the Smith Cloud filaments are consistent with them being part of a warm neutral medium within the cloud. It will be interesting to explore the distribution of filaments and filament temperatures further with future high resolution HI observations. Comparing Figures 2 and 3, we see that the GBT moment 0 map identifies material in the lower midsection, as well as the lower extending ridge. With higher-resolution data in the region not covered by GALFA-H I, *fil3d* would likely return filaments in these areas as well.

5.3 Overall Properties

The trends in velocity FWHM and column density in Figures 7 and 8 can be understood from the perspective that the farther out we look along this line of sight (represented at some level by the filament velocity) the greater the $|z|$ value from the plane becomes. With the FWHMs (and thereby temperatures from Equation 4), we see the local region has line widths consistent with the CNM but then scales to the WNM as $|z|$ increases as we reach the Smith Cloud, which sits 3 kpc below the disc. For column densities, we see the emission in the raw data peak around 0 km s^{-1} and drop off as we go further from the plane, which is consistent with the overall observed H I distribution of the Galactic ISM (Kalberla & Kerp 2009).

The separate filament groups also correspond to different physical scales. Assuming a distance of 200 pc, with the given GALFA-H I spatial resolution the local filaments have an average width (defined as twice the radial profile of the root node computed in *Filfinder*) of 0.66 pc, whereas at a distance of 12.4 kpc the HVC filaments have a mean width of 38 pc. These filaments are significantly larger than the sub-pc local ISM filaments and have not been studied as extensively in the literature. As such, their formation mechanism may vary from the smaller scale filaments and there may be multiple filaments embedded in the large linear structures.

Future work entails searching for filaments in other HVC complexes to see if properties are shared across different objects. For the Smith Cloud, in particular, a full high-resolution map is needed to study the filamentary structure of the entire cloud. An increased knowledge of the magnetic field of the Smith Cloud, as well as halo clouds in general, is also required to confirm the filaments align with the cloud’s magnetic field. It is also possible that filaments may exist in ionized hydrogen as well. The Smith Cloud has already been mapped in H- α (Hill et al. 2009) at a low resolution, but doing so at higher resolution may reveal a network of H- α filaments as seen in Galactic ISM H- α surveys (e.g. Homa et al. 2023).

ACKNOWLEDGEMENTS

The authors thank Susan Clark for many helpful discussions and Jay Lockman for sharing the GBT data of the Smith Cloud. This project makes use of NumPy (Harris et al. 2020), AstroPy (Astropy

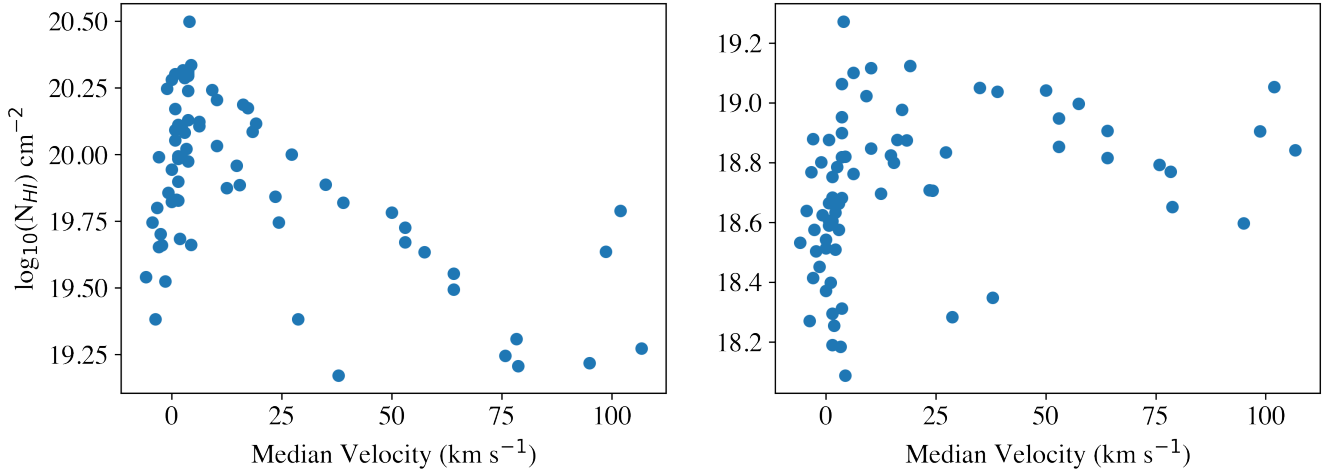


Figure 8. Median column density as a function of velocity for each filament generated from the raw (left) and USM (right) data. These distributions show the effect of the unsharp mask removing diffuse emission as well as the drop off in gas density with increasing distance from the disc along the line of sight.

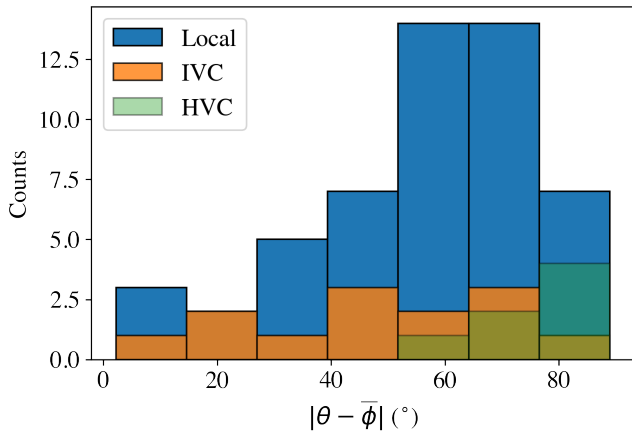


Figure 9. Histogram of filament alignment with the plane of sky magnetic field.

Collaboration et al. 2013, 2018), Matplotlib (Hunter 2007), *Filfinder* Koch & Rosolowsky (2015), and Healpy (Zonca et al. 2019)

DATA AVAILABILITY

This paper makes use of data from the Galactic Arecibo L Band Feed Array (GALFA) H I Data Release 2 which are publicly available to download at <https://purcell.ssl.berkeley.edu/>, the H I 4 π Survey, available at <http://cade.irap.omp.eu/dokuwiki/doku.php?id=hi4pi>, as well as observations from the *Planck* Collaboration, which are publicly accessible at <http://www.esa.int/Planck>. In addition, this paper made use of Smith Cloud data from the Robert C. Byrd Green Bank Telescope, Green Bank, WV, which is available upon reasonable request to the authors. Data and code corresponding to the plots in this paper are also available upon reasonable request to the authors.

REFERENCES

Alig C., Hammer S., Borodatchenkova N., Dobbs C. L., Burkert A., 2018,

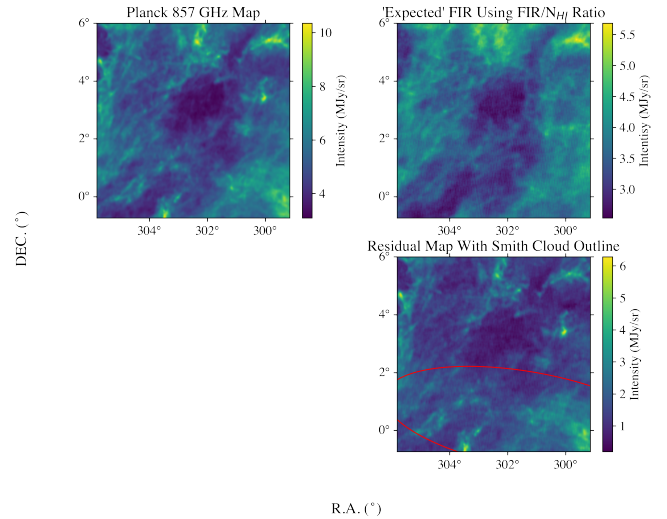


Figure 10. Top Left: The original *Planck* 857 GHz map in the region around the Smith Cloud. Top Right: The expected map created using column density map and the I_{857}/N_{H} ratio from Planck Collaboration et al. (2014). Bottom Right: Residual map, showing the expected map subtracted from the *Planck* map with the outline of the Smith Cloud included for reference.

ApJ, 869, L2

- André P., Di Francesco J., Ward-Thompson D., Inutsuka S. I., Pudritz R. E., Pineda J. E., 2014, in Beuther H., Klessen R. S., Dullemond C. P., Henning T., eds, *Protostars and Planets VI*. pp 27–51 ([arXiv:1312.6232](https://arxiv.org/abs/1312.6232)), [doi:10.2458/azu_uapress_9780816531240-ch002](https://doi.org/10.2458/azu_uapress_9780816531240-ch002)
- Astropy Collaboration et al., 2013, *A&A*, 558, A33
- Astropy Collaboration et al., 2018, *AJ*, 156, 123
- Betti S. K., Hill A. S., Mao S. A., Gaensler B. M., Lockman F. J., McClure-Griffiths N. M., Benjamin R. A., 2019, *ApJ*, 871, 215
- Bland-Hawthorn J., Veilleux S., Cecil G. N., Putman M. E., Gibson B. K., Maloney P. R., 1998, *MNRAS*, 299, 611
- Clark S. E., Hensley B. S., 2019, *ApJ*, 887, 136
- Clark S. E., Peek J. E. G., Putman M. E., 2014, *ApJ*, 789, 82
- Clark S. E., Hill J. C., Peek J. E. G., Putman M. E., Babler B. L., 2015, *Phys. Rev. Lett.*, 115, 241302
- Green D. A., 2015, *MNRAS*, 454, 1517

- HI4PI Collaboration et al., 2016, *A&A*, 594, A116
- Hacar A., Clark S. E., Heitsch F., Kainulainen J., Panopoulou G. V., Seifried D., Smith R., 2023, in Inutsuka S., Aikawa Y., Muto T., Tomida K., Tamura M., eds, *Astronomical Society of the Pacific Conference Series* Vol. 534, *Protostars and Planets VII*. p. 153 ([arXiv:2203.09562](https://arxiv.org/abs/2203.09562)), [doi:10.48550/arXiv.2203.09562](https://doi.org/10.48550/arXiv.2203.09562)
- Harris C. R., et al., 2020, *Nature*, 585, 357
- Heitsch F., Putman M. E., 2009, *ApJ*, 698, 1485
- Hill A. S., Haffner L. M., Reynolds R. J., 2009, *ApJ*, 703, 1832
- Hill A. S., Mao S. A., Benjamin R. A., Lockman F. J., McClure-Griffiths N. M., 2013, *ApJ*, 777, 55
- Homa J., Schiminovich D., Putman M., diCicco D., Walker S., Mittelman D., 2023, in *American Astronomical Society Meeting Abstracts*. p. 223.04
- Hunter J. D., 2007, *Computing in Science and Engineering*, 9, 90
- Jung S. L., Grønnow A., McClure-Griffiths N. M., 2023, *MNRAS*, 522, 4161
- Kalberla P. M. W., Kerp J., 2009, *ARA&A*, 47, 27
- Kalberla P. M. W., Kerp J., Haud U., Winkel B., Ben Bekhti N., Flöer L., Lenz D., 2016, *ApJ*, 821, 117
- Kim D. A., Clark S. E., Putman M. E., Li L., 2023, *MNRAS*,
- Koch E. W., Rosolowsky E. W., 2015, *MNRAS*, 452, 3435
- Lenz D., Hensley B. S., Doré O., 2017, *ApJ*, 846, 38
- Lockman F. J., Benjamin R. A., Heroux A. J., Langston G. I., 2008, *ApJ*, 679, L21
- Ma Y. K., et al., 2023, *MNRAS*, 521, 60
- Marasco A., Fraternali F., 2017, *MNRAS*, 464, L100
- McClure-Griffiths N. M., Dickey J. M., Gaensler B. M., Green A. J., Haverkorn M., 2006, *ApJ*, 652, 1339
- Nichols M., Bland-Hawthorn J., 2009, *ApJ*, 707, 1642
- Panopoulou G. V., et al., 2019, *ApJ*, 872, 56
- Peek J. E. G., Heiles C., Putman M. E., Douglas K., 2009, *ApJ*, 692, 827
- Peek J. E. G., et al., 2018, *ApJS*, 234, 2
- Planck Collaboration et al., 2014, *A&A*, 571, A11
- Planck Collaboration et al., 2020, *A&A*, 641, A3
- Putman M. E., Bland-Hawthorn J., Veilleux S., Gibson B. K., Freeman K. C., Maloney P. R., 2003, *ApJ*, 597, 948
- Putman M. E., Peek J. E. G., Jounge M. R., 2012, *ARA&A*, 50, 491
- Quilis V., Moore B., 2001, *ApJ*, 555, L95
- Shapiro P. R., Field G. B., 1976, *ApJ*, 205, 762
- Smith G. P., 1963, *Bull. Astron. Inst. Netherlands*, 17, 203
- Sofue Y., Kudoh T., Kawamura A., Shibata K., Fujimoto M., 2004, *PASJ*, 56, 633
- Soler J. D., et al., 2016, *A&A*, 596, A93
- Soler J. D., et al., 2020, *A&A*, 642, A163
- Soler J. D., et al., 2022, *A&A*, 662, A96
- Wakker B. P., York D. G., Wilhelm R., Barentine J. C., Richter P., Beers T. C., Ivezić Ž., Howk J. C., 2008, *ApJ*, 672, 298
- Zonca A., Singer L., Lenz D., Reinecke M., Rosset C., Hivon E., Gorski K., 2019, *The Journal of Open Source Software*, 4, 1298

APPENDIX A: ADDITIONAL SMITH CLOUD PLOTS

Here we show the ellipse used to represent the on/off boundary regions in the discussion of dust with respect to the Smith Cloud itself. The region was chosen to roughly correspond to $N_{\text{H}1} > 1 * 10^{20} \text{ cm}^{-2}$

This paper has been typeset from a $\text{T}_{\text{E}}\text{X}/\text{L}_{\text{A}}\text{T}_{\text{E}}\text{X}$ file prepared by the author.

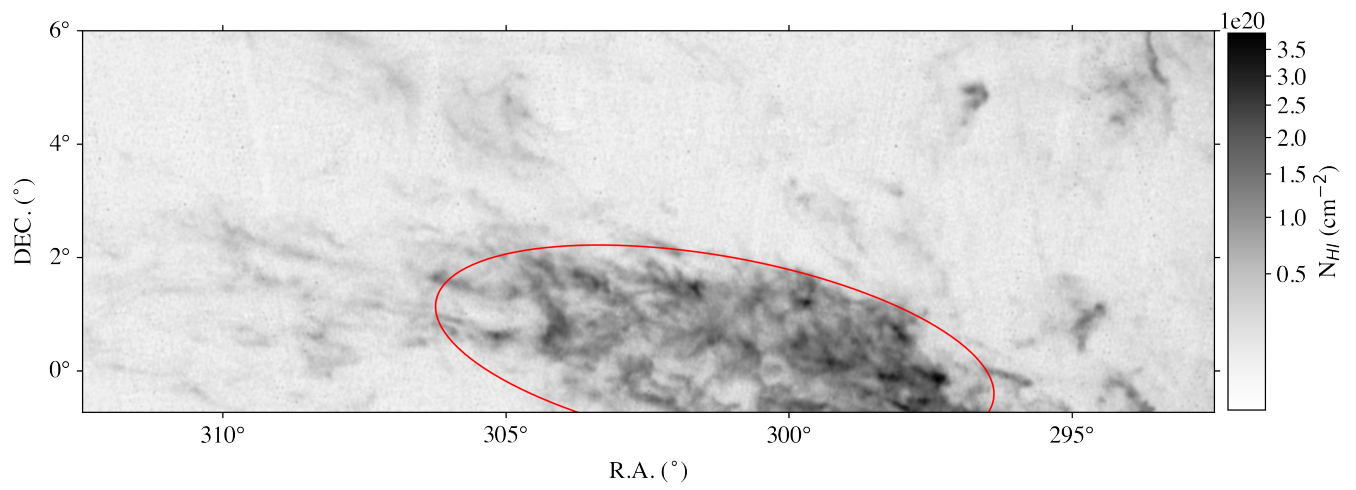


Figure A1. Ellipse used for sampling the potential presence of dust overlaid on the GALFA-H I column density map.